ISSN: 2277-9655
Scientific Journal Impact Factor: 3.449
(ISRA), Impact Factor: 1.852

IJESRT

INTERNATIONAL JOURNAL OF ENGINEERING SCIENCES & RESEARCH TECHNOLOGY

Analysis of Mechanism of Polarimetric Hyperspectral Imaging

Mrs. Supriya P. Gaikwad[*1], Prof. Vijay R. Dahake[2]
[*1]P.G Student, [2] Professor, Ramrao Adik Institute Of Technology, Nerul, Navi Mumbai-410210, India
supriya.nagane@gmail.com

Abstract

Hyperspectral imaging systems can acquire both spectral and spatial information of ground surface and have been used in a variety of applications. The work on polarimetric hyperspectral imaging mechanism and on image characteristics is of great importance for information extraction and utilization of the images. The purpose is to analyze the mechanism of polarimetric hyperspectral imaging and to model such a process.

The outcome will help designers and users of a polarimetric hyperspectral imaging system to further understand the system and take full advantages of it. Polarimetric hyperspectral images can provide spectral, spatial, and polarimetric information of a scene, which are unique and comprehensive for remote sensing applications such as growth monitoring of crops, analysis of water quality, and geology mapping, etc.

Here, a polarimetric hyperspectral imaging model is proposed, in which the influence of skylight on polarization is considered, Here we analyze and calculate the condition and parameters of the imaging models, the uniqueness, and usefulness of polarimetric and spectral information. Here we generate the polarimetric hyperspectral image data source according to the imaging model. The polarimetric hyperspectral image model is realized at the low attitude considering the characteristic of atmosphere environment.

Keywords: Imaging modeling, polarimetric hyperspectral images, polarimetric information.

Introduction

The modeling of hyperspectral imaging systems plays a number of roles in the development and application of the technology. One primary role is that by constructing and validating models, we demonstrate our understanding of the problematics and processes of hyperspectral imaging. Another major role is to create accurate simulations of hyperspectral images, which can be used as test imagery for algorithm development. A third role is to optimize the design and operation of the imaging systems by allowing trade off studies to characterize the impact of system parameter choices.Hyperspectral images possess spectral and spatial information of ground cover, which have been widely used in remote sensing fields. Polarimetric hyperspectral images can provide extra polarimetric information of a scene and are expected to play more important role than hyperspectral images in remote sensing applications such as monitoring growth status of vegetation [15], the atmosphere [16], and underwater ecological environment [17], etc.

The research on polarimetric hyperspectral imaging mechanism and on image characteristics is of great importance for further information extraction and utilization. In this project we analyze the mechanism of polarimetric hyperspectral imaging and model such a process. The outcome of the work can help system designers and users understand imaging process better and find the influencing factors to system performance, so as to optimize sensor parameters and to plan new missions.A great number of efficient and cost-effective data can also be produced for validation of hyperspectral data processing. As both sensor and processing systems become increasingly complex, the need for understanding the impact of various system parameters on performance also increases. Hyperspectral images contain a wealth of data, interpreting them requires an understanding of exactly what properties of ground materials we are trying to measure, and how they relate to the measurements actually made by the hyperspectral sensor.

Literature survey

In 1989, Kerekes and Landgrebe made a detailed description about the modeling and simulation of optical remote sensing system. Up to now, many models are developed to describe the reflection of vegetation canopies, such as AGR

ISSN: 2277-9655
Scientific Journal Impact Factor: 3.449
(ISRA), Impact Factor: 1.852

model [12], Suits model [6], etc. SAIL (scattering by arbitrary inclined leaves) is one of the earliest canopy reflectance models [7], gives rise to several improved versions. Kuusk put forward an improved SAIL model where the hot-spot effect was added [1]. Recently, Verhoef. proposed an extension of GeoSAIL including crown clumping, which was additiveally combined with PROSPECT(a model of leaf optical properties spectra) and a soil BRDF (bidirectional reflectance distribution function) model [14]. Fast canopy reflectance (FCR) model [9] overcomes the defect of SAIL model that failed considering the specular reflection on leaf surfaces and the hot-spot effect. The four-stream model is applied to describe the complex interaction of the heterogeneous and non-Lambertian land surface with the atmosphere in an effective manner. The six atmosphere parameters of four stream model can be calculated by MODTRAN4.0.

Vanderbilt and Grant firstly derived a specular reflectance and polarized reflectance model for the headed and preheaded plant canopy [19]. In 2005, Shell further analyzed three backgrounds and six targets polarization in his doctoral dissertation. In 2009, Waquet presented an alternative to the previous model by using a shadowing function given by Saunders, which assumed a Gaussian distribution of the surface slopes.

Method of implementation

This project proposes a polarimetric hyperspectral imaging model, in which the influence of skylight on polarization is considered.

First, three kinds of typical material's (vegetation, top soil, water surface) polarized reflectance models are analysed in detail. Next, we come up with a model of polarimetric hyperspectral imaging process based on the previous work of hyperspectral image modeling, and polarimetric information is characterized and introduced in the model. In contrast with the previous hyperspectral image modeling, however, the polarimetric hyperspectral image model here is realized at the low attitude considering the characteristic of atmosphere environment. Finally we also analyze the subpixel model.

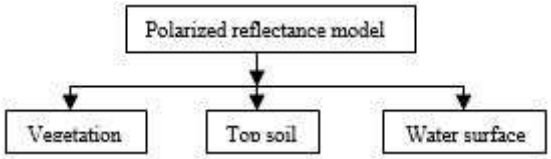

Figure 1. Implementation of polarized reflectance model.

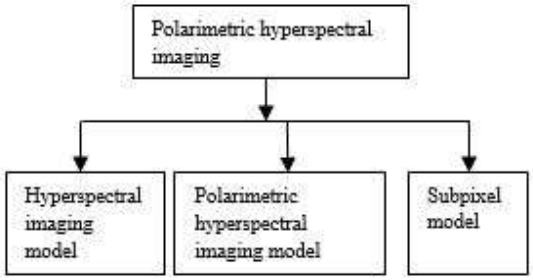

Figure 2. Implementation of polarimetric hyperspectral imaging.

Polarized reflectance model

Polarization mainly comes from the specular reflection of sunlight, although polarimetric information produced by skylight should not be ignored. Polarized radiance basically comes from the microcosmic surface's specular reflection, and these microcosmic surfaces are small Fresnel's reflectors with random orientation. As shown in Figure 3, it is evident that the microscopic normal and macroscopic normal are not consistent. When the ground target's surfaces are flat or near flat, their microscopic normals are almost parallel to the macroscopic normal. Under this condition, the microscopic normal often obeys a certain distribution function like Gaussian distribution, and the function's center is the macroscopic normal. More precisely, let S and dS stand, respectively, for macroscopic surface and for microcosmic surfaces whose direction of the normal is (μ_n, φ_n) within $d\omega_n$. dS represents the project of microcosmic surface dS_0. Then, the microcosmic surface's normal is characterized by the distribution function $p(\mu_n, \varphi_n)$ such that.

$$p(\mu_n, \varphi_n)\, d\omega_n = dS/S \quad \ldots\ldots(1)$$

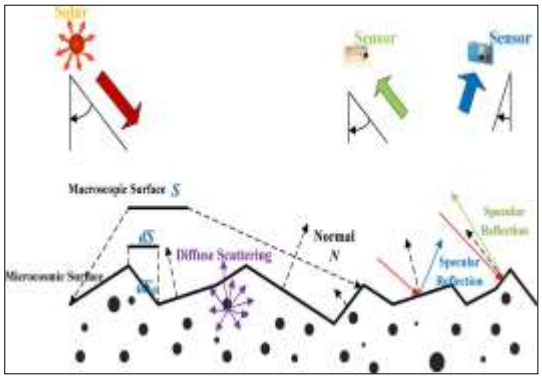

Figure 3. Propagation of light.

We can derive the polarized radiance L^{up} as,

$$L^{up} = \frac{E_p(\mu_n, \varphi_n)}{4\mu_v\mu_n} F_p(i, n) \quad \ldots\ldots(2)$$

And the value of polarized reflectance R_{pol} can be deducted by,

ISSN: 2277-9655
Scientific Journal Impact Factor: 3.449
(ISRA), Impact Factor: 1.852

$$R_{pol}(i) = \frac{\pi \times p(\mu_n, \varphi_n)}{4\mu_v\mu_n\mu_s} F_p(i,n) \ldots\ldots\ldots\ldots\ldots\ldots\ldots(3)$$

In general, $p(\mu_n, \varphi_n)$ can be regarded as a Gaussian function, $F_p(i,n)$ is Freshnel's polarized reflection coefficient. As the specular reflection is highly dependent on the types of material, surface roughness, etc., here we just consider the condition that surfaces are relatively flat; thus, the direction of surface's specular reflection is close to that of macroscopic normal's specular reflection. In this instance, when the microscopic normal is parallel to the macroscopic normal, incident light is reflected in the direction that reflected angle is equal to the incident angle; incident light and reflected light are within some plane according to Fresnel principle. This phenomenon is stochastic; the probability will gradually decrease when the microscopic normal is far from the macroscopic normal.

a) Case of vegetation:

A simple polarized reflectance model for vegetation canopy was proposed by Rondeaux and Herman in 1991. This model accounts for the leaf angle distribution and analyzes the effect of light transmission through the canopy. They pointed that the polarized reflectance is independent on the leaf area index for a dense canopy (LAI $\geq$ 3) Breon put forward a simpler version of the polarized reflectance model for vegetation canopy, which assumes a uniform leaf orientation and ignores the effect of LAI [3]. Leaf angle distribution function is generally defined as the probability density of leaf angle.

Breon's vegetation canopy model results are often lower than the measured data. Hence, we adopt the Rondeaux-Herman model in our work, and the effect of LAI is ignored.

b) Case of top soil:

A polarized reflectance model for bare soils was also given by Breon, using the hypothesis like that for vegetation canopy. Moreover, it does not consider attenuation of the incoming reflected rays within the depth of the canopy. The top soil model results are often higher than the measured data [4]. Waquet introduced a polarized reflectance model using a shadowing function, and this model fit not only for vegetation surface but for bare soils [11].

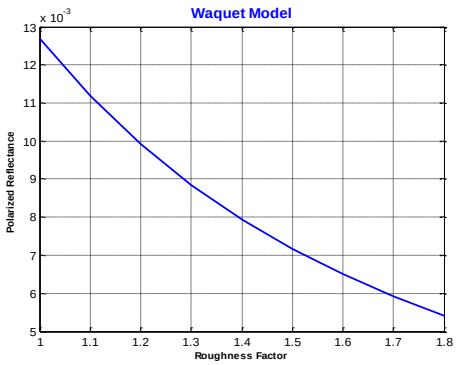

Figure 4. Waquet model

We can see that the polarized reflectance decreases with the increase of roughness factor. It is because the rougher the surface, the more severe attenuation of flux.

c) Case of water surface:

The water's polarized reflectance is affected by the waves, which depends on the wind speed. Hence, a wave facet's distribution function derived by Cox and Munk depends only on the wind speed ω and preserves the symmetry of the reflectance law [13]. The model assume that the entire water surface or some part of the land surface consists in small Fresnel's reflectors with random orientation.

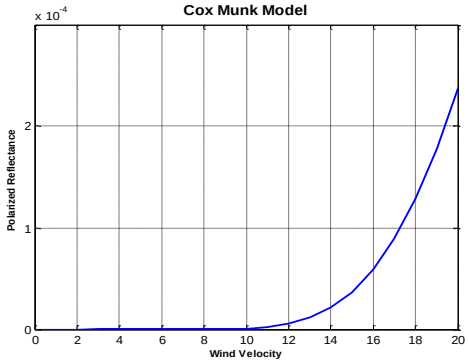

Figure 5. Cox-Munk model

We observe here that the value of polarized reflectance is also influenced by the climate, so the polarization can be utilized to monitor the weather change.

3.2 Polarimetric hyperspectral imaging

Based on our previous the hyperspectral simulation work, augments the polarization part. Therefore, we first analyze the hyperspectral imaging model and then put forward the polarimetric hyperspectral imaging model.

A) Hyperspectral imaging model:

In the modeling of hyperspectral imaging process, the four-stream radiance model [8] is

ISSN: 2277-9655
Scientific Journal Impact Factor: 3.449
(ISRA), Impact Factor: 1.852

adopted, in which major effects including heterogeneity of landscape, non- Lambertian reflectance of the land surface, atmospheric adjacency effect, and the limited spatial resolution of instrument are considered. The four-stream approximation is a reasonable tradeoff between real case and computational efficiency. In the model, the integral of equation needs to be determined to compute the radiance L_o of a surface element in observer's direction.

$$L_o(\mu_o,\varphi_o) = \rho(\mu_o,\varphi_o,\mu_s,\varphi_s)\, E_s(\mu_s,\varphi_s) + \int_0^{2\pi}\int_0^{1} \rho(\mu_o,\varphi_o,\mu_i,\varphi_i)\, L_i(\mu_i,\varphi_i)\, \mu_i d\mu_i d\varphi_i \ldots\ldots..(4)$$

where L_o is the radiance to the observer, ρ is the four dimensional BRDF, Es is the direct solar irradiance on a horizontal plane, μ (cosine of the zenith angle) and φ (azimuth) are directional arguments for directions signed by subscripts: s (from the sun), i (from the sky), and o (to the observer). According to the four-stream radioactive transfer theory, the radiance Lo received by the sensor can be computed as,

$$L_o = \rho_{so}\frac{E_s^o}{\pi}\cos\theta_s + \frac{\tau_{ss}\bar{r}_{sd}+\tau_{sd}\bar{r}_{dd}}{1-\bar{r}_{dd}\rho_{dd}}\tau_{do}\frac{E_s^o}{\pi}\cos\theta_s + \frac{\tau_{sd}+\tau_{ss}\bar{r}_{sd}\rho_{dd}}{1-\bar{r}_{dd}\rho_{dd}}\, r_{do}\tau_{oo}\frac{E_s^o}{\pi}\cos\theta_s + \tau_{ss}r_{so}\tau_{oo}\frac{E_s^o}{\pi}\cos\theta_s \ldots\ldots\ldots\ldots..(5)$$

where r_{so} is target bidirectional reflectance, r_{do} is target directional reflectance for diffuse incidence, r_{sd} is the average surroundings diffuse reflectance for solar incidence, r_{dd} is the average surroundings diffuse reflectance for diffuse incidence, ρ_{so} is the bidirectional reflectance at the top of atmosphere, ρ_{dd} is the spherical albedo at the bottom of atmosphere (BOA), τ_{ss} is the direct atmospheric transmittance in the direction of the sun, τ_{oo} is the direct atmospheric transmittance in the direction of viewing, τ_{sd} is the diffuse atmospheric transmittance for solar incidence, τ_{do} is the directional atmospheric transmittance for diffuse incidence, E_{os} is the direct solar irradiance on a plane perpendicular to the sunrays, and θ_s is the local solar zenith angle.

According to the theory of Verhoef's four stream model, we rederive the model again.

The six atmosphere parameters calculated are,

$$\tau_{ss} = \exp(-b/\cos\theta_s)\ldots\ldots\ldots\ldots\ldots\ldots\ldots(6)$$

$$\tau_{oo} = \exp(-b/\cos\theta_o)\ldots\ldots\ldots\ldots\ldots\ldots\ldots(7)$$

$$\tau_{ss}\tau_{oo} = \exp[-b(1/\cos\theta_s + 1/\cos\theta_o)] = GSUN_{100}\times\pi/(E_s^o\cos\theta_s)\ldots\ldots\ldots\ldots(8)$$

$$\rho_{so} = PATH_o\times\pi/(E_s^o\cos\theta_s)\ldots\ldots\ldots\ldots(9)$$

$$\tau_{sd} = \left[\frac{GTOT_{100}(1-\rho_{dd})}{GSUN_{100}} - \rho_{dd}\right]\tau_{ss}\ldots\ldots(*)(10)$$

$$\tau_{do} = \frac{PATH_{100}-PATH_0}{GTOT_{100}}\cdot\frac{\tau_{sd}+\tau_{ss}\rho_{dd}}{\tau_{sd}+\tau_{ss}}\tau_{oo}\ldots\ldots\ldots(*)(11)$$

$$\rho_{dd}^2\left(\frac{GTOT_{50}}{GTOT_{100}}-\frac{1}{2}\right)\tau_{ss} + \rho_{dd}\left[\frac{\tau_{ss}}{2}-\tau_{sd}+(\tau_{sd}-2\tau_{ss})\cdot\frac{GTOT_{50}}{GTOT_{100}}\right] + \left(1-2\cdot\frac{GTOT_{50}}{GTOT_{100}}\right)\cdot\tau_{sd} = 0\ldots\ldots\ldots\ldots(*)(12)$$

Where b is the extinction coefficient representing the optical thickness of the atmospheric layer, and θ_o is the zenith angle of observation. $GTOT_0$, $GTOT_{50}$, and $GTOT_{100}$ are spectrally flat surface albedos of 0%, 50%, and 100%, respectively, here all for a uniform Lambertian surface reflectance. The three revised parameter equations are labelled by (∗) including the diffuse atmospheric transmittance for solar incidence τ_{sd}, the directional atmospheric transmittance for diffuse incidence τ_{do}, and the BOA spherical albedo of the atmosphere ρ_{dd}. After the six atmosphere parameters are obtained, and the four directional reflectance parameters also can be calculated. The results of six atmosphere parameters are shown in Fig. 7.

B) Polarimetric hyperspectral imaging model:

Polarized radiance mainly depends on the specular reflection of sunlight; thus, conventional surface polarized radiance model does not take the skylight into consideration. However, the contribution of skylight for polarized radiance cannot be ignored. According to the data which is obtained [5], the ratio of polarized radiance which is produced by skylight is in the range of 10%–20%. Therefore, we need to integrate the polarized radiance from skylight.

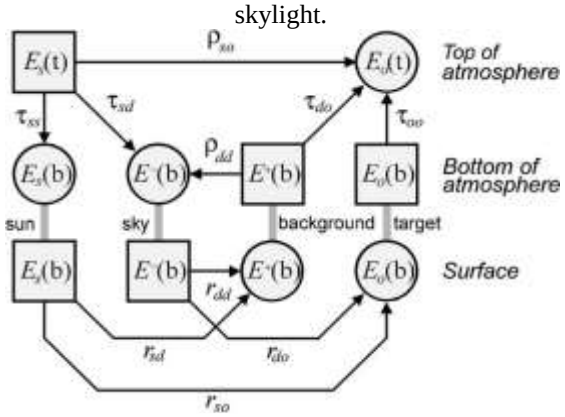

ISSN: 2277-9655
Scientific Journal Impact Factor: 3.449
(ISRA), Impact Factor: 1.852

Figure 6. Flux-interaction diagram of the atmosphere over a non-Lambertian reflecting earth's surface.

By means of a flux-interaction diagram, the radiative transfer inside the atmosphere and the non-Lambertian reflection at the earth's surface can be summarized as in Figure 6. According to the four-stream model, the total radiance received by sensor is L_o. Then, the total radiance is divided into five parts which are path radiance, adjacent radiance, ref-sun radiance, ref-multi-skylight radiance, and ref-rayleigh radiance. The "ref-" means that the ground target reflects incident light, and incident light may be sunlight(ref-sun), or multiple scattering skylight (ref-multi-skylight), or skylight from Rayleigh scattering(ref-rayleigh).

$$L_o = L_{path} + L_{adjacent} + (L_{mul-scattering} \cdot r_{do} + L_{reyleigh} \cdot r_{do} + L_{sun} \cdot r_{so})\tau_{oo} \quad \text{.....(13a)}$$

$$L_o = \rho_{so}\frac{E_s^o}{\pi}\cos\theta_s + \frac{\tau_{ss}\bar{r}_{sd} + \tau_{sd}\bar{r}_{dd}}{1-\bar{r}_{dd}\rho_{dd}}\tau_{do}\frac{E_s^o}{\pi}\cos\theta_s + \frac{\tau_{sd}\bar{r}_{dd} + \tau_{ss}\bar{r}_{sd}}{1-\bar{r}_{dd}\rho_{dd}}\rho_{dd}\frac{E_s^o}{\pi}\cos\theta_s \cdot r_{do}\tau_{oo} + \tau_{sd}\frac{E_s^o}{\pi}\cos\theta_s \cdot r_{do}\tau_{oo} + \tau_{ss}\frac{E_s^o}{\pi}\cos\theta_s \cdot r_{so}\tau_{oo} \quad \text{.....(13b)}$$

Where, L_{path} and $L_{adjancet}$ received by sensor, are path radiance and adjacent radiance. $L_{mul-scattering}$, $L_{rayleigh}$, and L_{sun} are radiances from multiple scattering skylight, skylight from rayleigh scattering, and sunlight that irradiate into the target.

Moreover, it is reasonable that Waquet ignores the path polarized radiance and adjacent polarized radiance when the weather is "no rain, no cloud," and the altitude of sensor is lower than 35 km. The atmospheric polarized radiance can be accurately estimated using the successive order of scattering code. To simplify, we also ignore the path polarized radiance and adjacent polarized radiance. Therefore, in terms of polarized radiance, we just consider that the polarized radiance comes from ground targets.

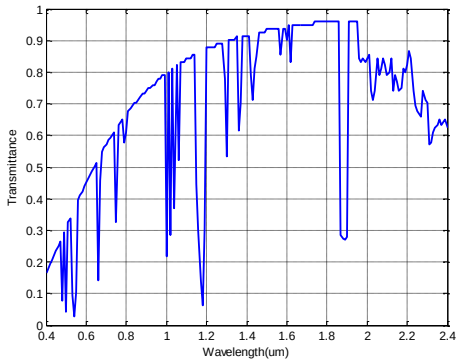

(a)

Figure 7. Six atmosphere parameters (a) τ_{ss} (b) τ_{oo} (c) ρ_{so} (d) τ_{sd} (e) τ_{do} (f) ρ_{dd}.

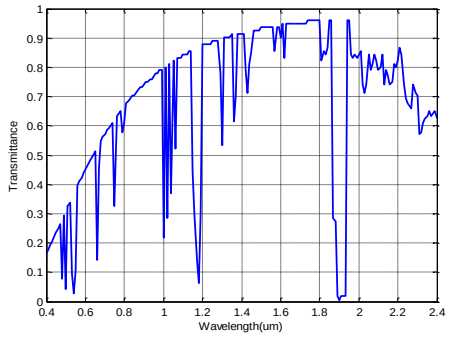

(b)

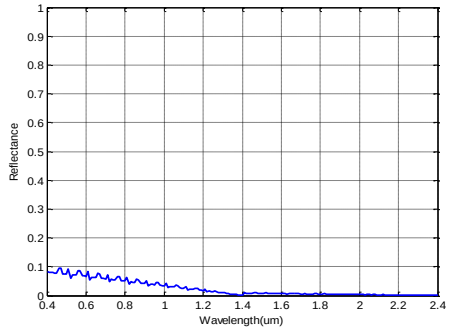

(c)

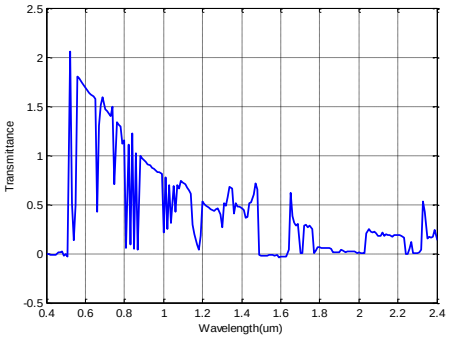

(d)

ISSN: 2277-9655
Scientific Journal Impact Factor: 3.449
(ISRA), Impact Factor: 1.852

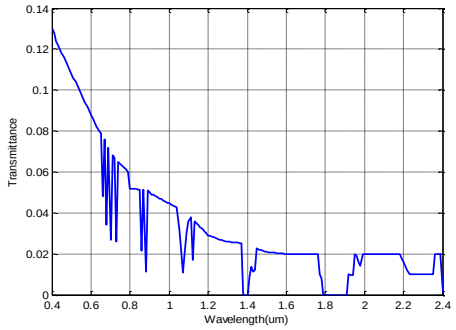

(e)

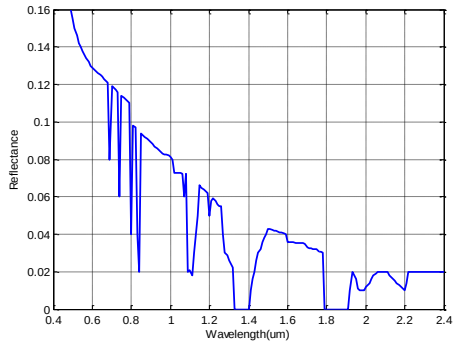

(f)

C) Subpixel Model:

Here, a simple area-weighted linear mixing model is used to obtain the reflectance of pixels in woodland-road scene that contains two classes (shrubbery and uncovered soil). Particularly, for cylindrical and spherical plant crown, according to the interaction between the crown and ground surface geometric-optical characteristics, four ground surface fractions can be decided. A pixel is modeled as an area-weighted sum of the reflectance of the four scene components: sunlit ground, sunlit crown, shadowed ground, and shadowed crown. The reflectance of mixed pixel in the scene depends on the four parameters, i.e., f_C for sunlit crown, f_T for shadowed crown side, f_G for sunlit ground, and f_Z for shadowed ground. The four subpixel parameters are used to describe the proportion of the four representative scene components, respectively, which are influenced by solar zenith angle, viewing zenith angle, and tree density per resolution element in the scene. This subpixel model has been described [18].

1) Directional Reflectance Parameters: For the subpixel model, the directional reflectance r_{so}, r_{do}, r_{sd}, and r_{dd} are,

$$r_{so} = f_C\rho_c(\mu_o, \varphi_o, \mu_s, \varphi_s) + f_G\rho_s(\mu_o, \varphi_o, \mu_s, \varphi_s) \quad \text{.....(14)}$$

$$r_{do} = \frac{1}{\pi}\int_0^{2\pi}\int_0^1[(f_C + f_T)\rho_c(\mu_o, \varphi_o, \mu_i, \varphi_i) + (f_G + f_Z)\rho_s(\mu_o, \varphi_o, \mu_i, \varphi_i)]\,\mu_i d\mu_i d\varphi_i \quad \text{....(15)}$$

$$r_{sd} = \frac{1}{\pi}\int_0^{2\pi}\int_0^1[f_C\rho_c(\mu_i, \varphi_i, \mu_s, \varphi_s) + f_G\rho_s(\mu_i, \varphi_i, \mu_s, \varphi_s)]\,\mu_i d\mu_i d\varphi_i \quad \text{.....(16)}$$

$$r_{dd} = \frac{1}{\pi^2}\int_0^{2\pi}\int_0^1\int_0^{2\pi}\int_0^1[(f_C + f_T)\rho_c(\mu_o, \varphi_o, \mu_i, \varphi_i) + (f_G + f_Z)\rho_s(\mu_o, \varphi_o, \mu_i, \varphi_i)] \times \mu_i\mu_o d\mu_i d\varphi_i d\mu_o d\varphi_o \quad \text{.....(17)}$$

The foliage's reflectance $\rho_c(\mu_o, \varphi_o, \mu_s, \varphi_s)$ is realized by FCR model. The soil can be seen as Lambertian surface, whose reflectance $\rho_s(\mu_o, \varphi_o, \mu_s, \varphi_s)$ can be obtained from the spectrum database.

The results of four directional reflectance parameters are shown in Fig. 8. Thus, four directional reflectance parameters and six atmosphere parameters are derived and we modify these parameters to get the better results. Therefore, with these four directional reflectance parameters and six atmosphere parameters we obtain the total radiance that is received by the sensor.

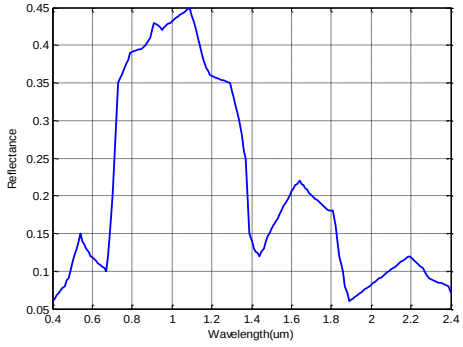

(a)

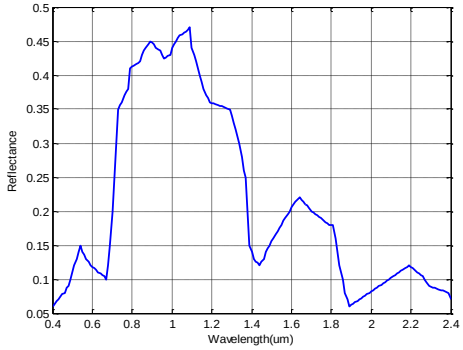

(b)

ISSN: 2277-9655
Scientific Journal Impact Factor: 3.449
(ISRA), Impact Factor: 1.852

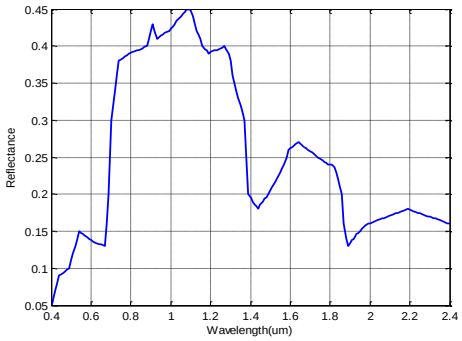

(c)

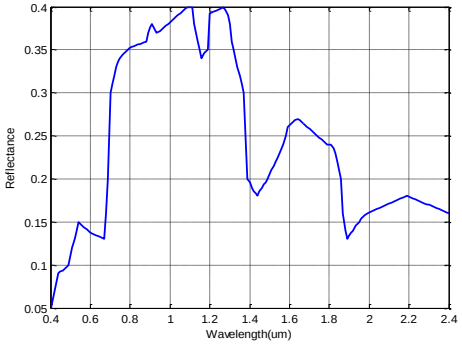

(d)

Figure 8 four directional reflectance parameters (a) r_{so} (b) r_{do} (c) r_{sd} (d) r_{dd}.

Future scope

The outcome of the work help designers and users of a polarimetric hyperspectral imaging system to optimize sensor parameters and plan new missions. Polarimetric hyperspectral imaging can be used for growth monitoring of crops, analysis of water quality, and geology mapping, etc.

The researches on polarimetric hyperspectral imaging mechanism and on image characteristics are of great importance for further information extraction and utilization of the images. The mapping of vegetation, water content is another emerging application for forest fire risk assessment, and forest defoliation resulting from heat waves, insect or fungus infections. In future more data modelling for better understanding of the interactions between the actively or naturally emitted radiance and the forest, a challenge is to understand interactions under various conditions.

Conclusion5

We study the polarimetric hyperspectral imaging model to realize the ideal and real scene implementation of polarimetric hyperspectral image. We modify the Verhoef's six atmosphere parameters, and the influence of skylight on polarization is analysed and four directional reflectance parameters are derived. Finally, we generate the polarimetric hyperspectral image data source according to the imaging model.

Polarization is independent of the spectral feature. The polarization can provide the supplementary information for the image interpretation other than spectral and spatial features. Polarimetric hyperspectral remote sensing combines the advantages of polarization and hyperspectral techniques.

References

[1] Kuusk, "A multispectral canopy reflectance model," Remote Sens. Environ., vol. 50, no. 2, pp. 75–82, Nov. 1994.

[2] G. Rondeaux and M. Herman, "Polarization of light reflected by crop canopies," Remote Sens. Environ., vol. 38, no. 1, pp. 63–75, Oct. 1991.

[3] F. M. Bréon, D. Tanre, P. Lecomte, andM. Herman, "Polarized reflectance of bare soils and vegetation measurements and models," IEEE Trans. Geosci. Remote Sens., vol. 33, no. 2, pp. 487–490, Mar. 1995.

[4] F. Maignan, F. M. Breon, E. Fedele, and M. Bouvier, "Polarized reflectances of natural surfaces: Spaceborne measurements and analytical modeling," Remote Sens. Environ., vol. 113, no. 12, pp. 2642–2650, Dec. 2009.

[5] J. R. Shell, "Polarimetric remote sensing in the visible to near infrared," Ph.D. dissertation, Rochester Inst. Technol., Rochester, NY, 2005, pp. 1–259.

[6] G. H. Suits, "The calculation of the directional reflectance of a vegetation canopy," Remote Sens. Environ., vol. 2, pp. 117–125, 1972.

[7] W. Verhoef, "Light scattering by leaf layers with application to canopy reflectance modeling: The SAIL model," Remote Sens. Environ., vol. 16, no. 2, pp. 125–141, Oct. 1984.

[8] W. Verhoef and H. Bach, "Simulation of hyperspectral and directional radiance images using coupled biophysical and atmospheric radiative transfer models," Remote Sens. Environ., vol. 87, no. 1, pp. 22–41, Sep. 2003.

[9] A. Kuusk, "A fast, invertible canopy reflectance model," Remote Sens. Environ., vol. 51, no. 3, pp. 342–350, Mar. 1995.

[10] T. Nilson and A. Kuusk, "A reflectance model for the homogeneous plant canopy

ISSN: 2277-9655
Scientific Journal Impact Factor: 3.449
(ISRA), Impact Factor: 1.852

and its inversion," Remote Sens. Environ., vol. 27, no. 2, pp. 157– 167, Feb. 1989.

[11]F. Waquet, J.-F. Leon, B. Cairns, and P. Goloub, "Analysis of the spectral and angular response of the vegetated surface polarization for the purpose of aerosol remote sensing over land," Appl. Opt., vol. 48, no. 6, pp. 1228– 1236, Feb. 2009.

[12]W. A. Allen, T. V. Gayle, and A. J. Richardson, "Plant canopy irradiance specified by the Duntley equations," J. Opt. Soc. Amer., vol. 60, no. 3, pp. 372–376, Mar. 1970.

[13]J. Lenoble, M. Herman, and J. L. Deuze, "A successive order of scattering code for solving the vector equation of transfer in the earth's atmosphere with aerosols," J. Quant. Spectrosc. Radiat. Transf., vol. 107, no. 3, pp. 479–507, Oct. 2007.

[14]S. Jacquemoud, W. Verhoef, F. Baret, C. Bacour, P. J. Zarco-Tejada, G. P. Asner, C. François, and S. L. Ustin, "PROSPECT+SAIL models: A review of use for vegetation characterization," Remote Sens. Environ., vol. 113, no. 1, pp. S56–S66, Sep. 2009.

[15]V. C. Vanderbilt and L. Grant, "Plant canopy specular reflectance model," IEEE Trans. Geosci. Remote Sens., vol. GRS-23, no. 5, pp. 722–730, Sep. 1995.

[16]F. Vachon, A. Royer, M. Aube, B. Toubbé, N. T. O'Neill, and P.M. Teillet, "Remote sensing of aerosols over North American land surfaces from POLDER and MODIS measurements," Atmos. Environ., vol. 38, no. 21, pp. 3501–3515, Jul. 2004.

[17]A. Tonizzo, J. Zhou, and A. Gilerson, "Polarized light in coastal waters: Hyperspectral and multiangular analysis," Opt. Exp., vol. 17, no. 7, pp. 5666–5683, Mar. 2009.

[18]J. Zhang, X. Zhang, B. Zou, and D. Chen, "On hyperspectral image simulation of a complex woodland area," IEEE Trans. Geosci. Remote Sens., vol. 48, no. 11, pp. 3889–3902, Nov. 2010.

[19]V. C. Vanderbilt, "A model of plant canopy polarization response," Purdue Libraries, West Lafayette, IN, LARS Tech. Rep., pp. 98–108, 1980.